Original Article

Azhar M. Memon*, Umar T. Salman, Abdulhammed K. Hamzat and Luai M. AlHems

Neural network method for the modeling of SS 316L elbow corrosion based on electric field mapping

https://doi.org/10.1515/corrrev-2021-0057
Received July 14, 2021; accepted February 16, 2022;
published online May 19, 2022

Abstract: Stainless steel is known for its superior corrosion resistance in industrial applications. In this work, corrosion modeling of stainless steel 316L is presented using artificial neural networks. The experimental setup consists of a loop containing stainless steel elbow with simulated seawater of known concentration continuously flowing at a specific flow rate, thus allowing to study the effect of flow dynamics and salt concentration on corrosion. Electric field mapping setup is used to collect the voltage and current information along with the temperature of the elbow section. In addition to modeling, characteristics of the observed scale deposits are also studied in-depth and briefly reported in this work.

Keywords: corrosion modeling; electric field mapping; neural networks; scale deposition; SS 316L elbow.

1 Introduction

Pipelines form essential infrastructure of multiple industries and facilities for the transportation of fluids. They are used in nuclear power plants, hydroelectric stations, food processing, oil and gas, and marine industries. Corrosion, cracks, and defects are usually responsible for the failure of a pipeline which can lead to serious safety issues such as leakages, personnel injury, fatalities, environmental degradation, and economic impacts like expensive repairs, costly outage, and production downtime. Owing to such a magnitude of impacts, it is vital to ensure stringent asset integrity protocols by regular inspection and maintenance. Therefore, inspection, evaluation, modelling, and prediction of corrosion in pipelines have become major research areas in academia and industry; see for example Vanaei et al. (2017), Heidary et al. (2018), Papavinasam et al. (2006), and Xie and Tian (2018), and references therein.

The service life of pipelines is greatly reduced by corrosion, which can be of several types such as, uniform or general (Choi et al. 2011), pitting, crevice, intergranular, erosion–corrosion (E–C), corrosion due to microbial growth, and environment induced cracking. This paper focuses on modeling and prediction of E–C using neural networks (NNs) in stainless steel (SS) elbow due to the flowing saline solution. Although SS is a costly and heavy alloy, the advantages of using it in certain applications and industries outperform the disadvantages. These include availability of a wide variety of types and grades providing flexibility of application, resistance to corrosion and UV radiation, durability, strength, being food-grade, and a good choice for high-temperature settings, making them a preference in many areas. These include food and beverage industry as it is resistant to microbial growth and does not react with the food, and wastewater treatment equipment due to the ease of cleaning. Another interesting advantage for the industry is that the SS equipment holds its resale value in case the operational needs change or the plant needs to be salvaged. In what follows, a concise literature review is given for the highlighted works related to E–C in SS.

Corrosion rate can be significantly reduced with the formation of a thin passive film on SS surface. However, due to the impingement of sand or other abrasive particles in the fluid on SS surface would lead to removal of these films, thus enhancing corrosion remarkably. This phenomenon is referred to as E–C, and this could lead to severe

***Corresponding author: Azhar M. Memon**, Applied Research Center for Metrology, Standards and Testing, Research Institute, King Fahd University of Petroleum and Minerals, Dhahran 31261, Saudi Arabia, E-mail: azhar.memon@kfupm.edu.sa. https://orcid.org/0000-0003-0982-2265
Umar T. Salman, Electrical Engineering Department, King Fahd University of Petroleum and Minerals, Dhahran 31261, Saudi Arabia
Abdulhammed K. Hamzat, Mechanical Engineering Department, King Fahd University of Petroleum and Minerals, Dhahran 31261, Saudi Arabia
Luai M. AlHems, Applied Research Center for Metrology, Standards and Testing, Research Institute, King Fahd University of Petroleum and Minerals, Dhahran 31261, Saudi Arabia

wall thinning if combined with the dynamics of fluid flow. Moreover, E–C can produce higher wall penetration rates than erosion or corrosion alone. In this context, Zeng et al. (2018) studied the semiconductivities of passive films at SS 304 elbow in sand-containing saline solution through a loop system. The solution contained 3.5 wt% NaCl with 0.9 wt% sand particles (size of 400–500 μm). The effects of fluid dynamics at the elbow on semiconductivities and compositions (using spectroscopy) of passive films were described. Shadley et al. (1996) presented E–C of carbon steel (CS) elbow as part of the flow loop, in a CO2 environment with sand particles. Depending on the fluid velocity, three E–C characteristics were found: protective scales formation at low velocities resulting in low corrosion rates, prevention of scales formation at higher velocities giving higher and uniform corrosion rates, and at intermediate velocities localized points with deep pits were observed along with over-all formation of protective scales. In addition, a computational model was given for the prediction of sand erosion in pipes. The levels of environmental conditions beyond which E–C becomes significant in predicting pipeline material thickness loss were studied by Hu and Neville (2009). Specifically, pipeline steel (API X65) degradation was reported due to E–C with fluid containing sand in a CO2 saturated environment. E–C prediction was enhanced by supplementing the empirical, amechanistic, and computational models with the environmental or external factors such as fluid flow velocity, temperature, and solid loading.

A study which compared the E–C behavior of CS 1018 and SS 304L was given in Khan et al. (2019), for 90° long radius elbows under slug flow conditions with sand particles. The results showed a lower surface roughness for SS compared with CS, four times higher E–C rate for CS than SS elbow, and higher E–C rate on the upper half of the elbow compared to the bottom half for both materials. Therefore, concluding that SS has superior corrosion resistance properties compared with CS.

Corrosion prediction for SS 316L was reported in Wan and Saito (2018) under flow-accelerated corrosion (FAC). A mass transfer study was performed by incorporating a corrosion model in the CFD analysis. The prediction results for pipe segments with abruptly varying diameters were in conformance with the measured ones. However, for the uniform part, the predicted corrosion depth was about 1.3 to 3.5 times the average experimental corrosion depth.

To the best of authors' knowledge, a comprehensive artificial NN (ANN) model for the complex process of corrosion and passive layer formation inside SS 316L elbow with consideration of flow dynamics and water salinity is lacking in the literature. In this spirit, this paper presents first results of such modelling for wall thinning in SS 316L elbow as part of a loop running saline water with known concentration and flow velocity. The measurement setup consisted of electric field mapping (EFM) pins to measure voltage and current readings, and temperature sensors. These readings were used to train an ANN to model the corrosion behavior and the performance was tested. A detailed chemical and microscopic analysis of scales formed on the internal surface was also performed, and is concisely described in this paper.

2 Experimental setup

The setup consists of a state-of-the-art flow loop that is designed to simulate real-time industrial conditions. The experimental setup, schematic, and columns layout are shown in Figure 1. It consists of two centrifugal pumps from Lowara Company, model number TG334, flow rate (Q) 45 m^3/h, head (h) 110 m, OMEGA turbine flow meter (FTB730), power switch (Eurotherm 2500P Schneider Electric), Plexiglass pipe section to visually examine the flow condition, and elbow section of SS 316L. This section is 3.01 m long with 4 in internal diameter and a nominal wall thickness (WT) of 6.03 mm. The flow inlet and outlet arms of the elbow are 1.2 and 1.25 m long (including 0.6 m long Plexiglass), respectively. Inlet arm, elbow section, and outlet arm of the pipe elbow are all made of corrosion resistant SS 316L.

EFM monitor which consists of an array of nonintrusive sensing pins, are permanently attached to the elbow's surface in the matrix of 16 columns and 7 rows, i.e., a total of 112 pins, as illustrated in Figure 1(c). These pins do not penetrate the pipe due to being nonintrusive. A measured amount of excitation current is injected into the structure and simultaneous measurements of the voltage pattern are recorded through these pins. The collected data consists of a time-series of differential pin voltages (in μV) and the corresponding array of current shunt measurements (in Amperes). The resistance of a volume is inversely related to the WT, i.e., a thinner wall will present a higher resistance to current flow and therefore generate a higher voltage drop for the same amount of excitation current. Due to temperature variations resulting from the fluid flow and ambient conditions, an additional temperature compensation step is required to account for the change in the resistivity. This is accomplished with additional pins for temperature measurements. The setup has the provision of reading electrical data and compute the remaining WT of the elbow section, however, this calculation software is not

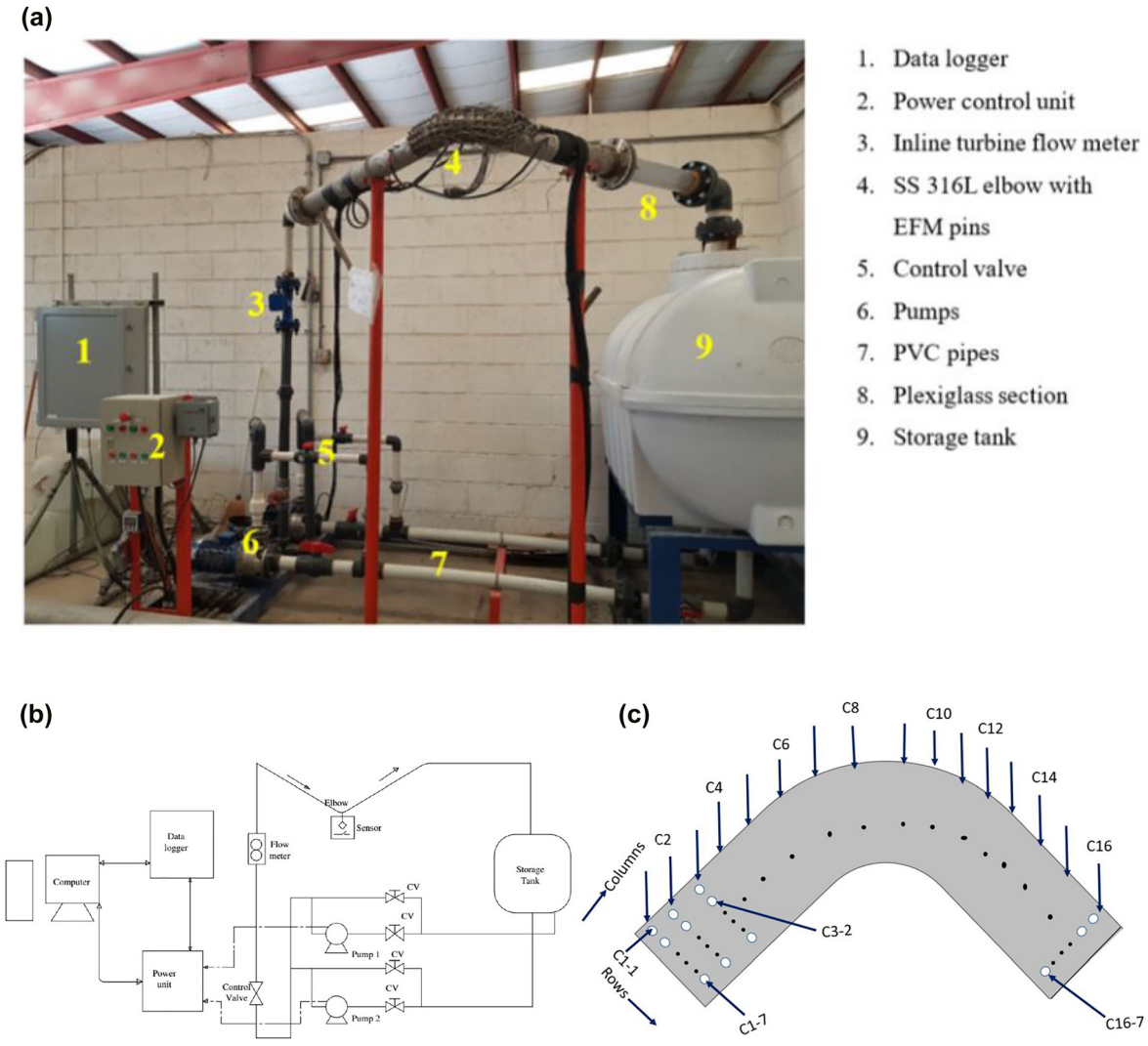

Figure 1: Mini flow loop.
(a) Experimental facility, (b) Schematic diagram, and (c) Illustration of the elbow pipe showing positions of 16 columns by 7 rows pin positions.

provided by the manufacturer. The data is uploaded to their server, where after several weeks, all calculations are done and the WT results are provided. This limitation formed the main motivation to develop a local NN based model to provide WT readings, in relatively less time, from the available voltage, current and temperature readings.

3 Materials and methods

To evaluate the impact of simulated seawater on corrosion and scale deposit, pure dried vacuum (PDV) salt was dissolved well in 1 m^3 of tap water (without sand). Handheld refractometer (REF234) was used to measure the salinity of the prepared solution, with three concentrations: 3.0, 3.5, and 4.0%. The fluid was supplied from a 2 m^3 storage tank, as shown in Figure 1(a), and circulated using both centrifugal pumps which gave a maximum combined flow rate of 70 m^3/hr. Control valves were used to regulate the flow rates at the pump entrance and exit. The rates and total flow pumped was measured using an inline turbine flow meter.

Experimental data consisted of hourly recorded differential voltage (ΔV), differential current (ΔI), temperature (T), and baseline reading of the pipe WT measured with ultrasonic testing (UT) probe at the beginning. The manufacturer's server was also fed with this pipe thickness reading before the start of the experiment. The ANN was trained with ΔV, ΔI and T as input and the pipe WT returned from the manufacturer's analysis software as output data. UT probing at the end of the experiment showed increased WT due to scale formation and decrease in WT after scale removal from the pipe, which are described below.

3.1 Scale formation

Spectroscopic analysis was carried out on the scale deposit sample extracted from the pipe during cleaning. The composition of water run

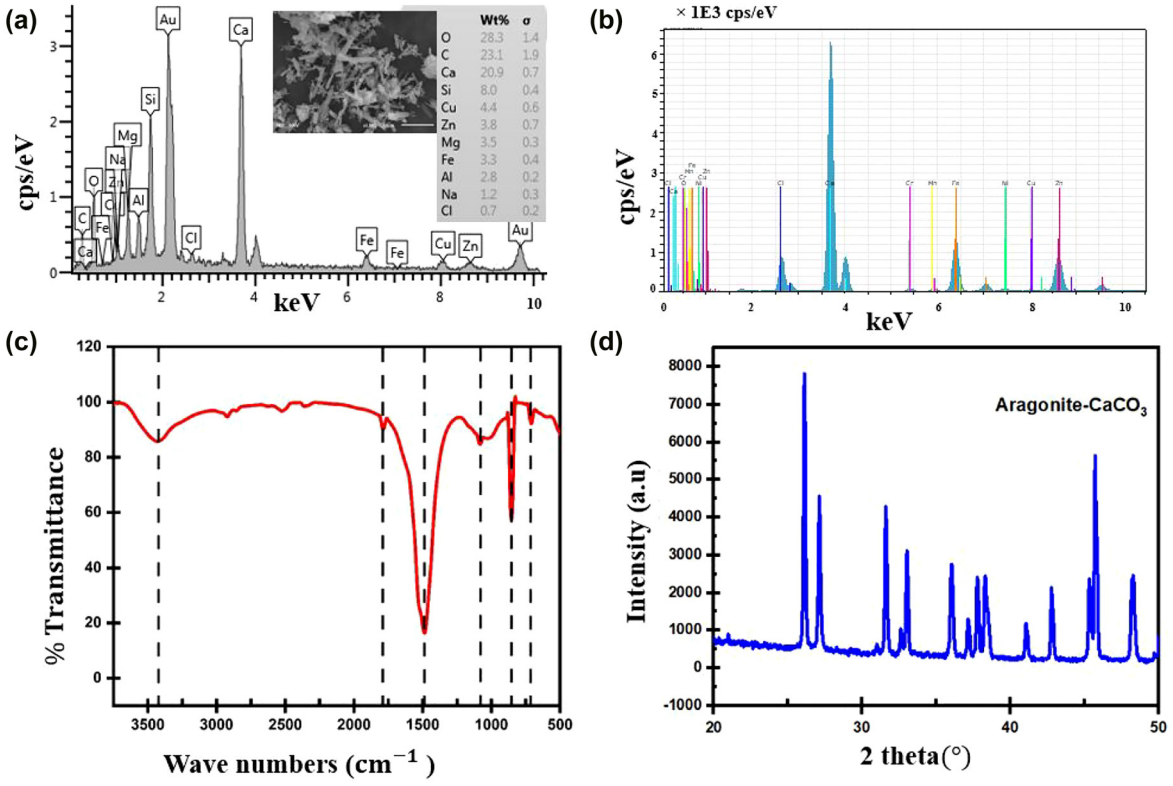

Figure 2: Spectroscopic analysis of extracted scale deposit (a) SEM-EDS (b) XRF (c) FT-IR (d) XRD.

through the system was found responsible for the formation of scale as it contained Calcium with a concentration of 291 mg/L. Figure 2(a) shows the percentage elemental composition of the extracted sample obtained from scanning electron microscopy with energy dispersive spectroscopy (SEM-EDS) characterization, whereas X-ray fluorescence showing the oxide state of the elements (not captured with EDS analysis) is indicated in Figure 2(b). Fourier-transform infrared spectroscopy (FT-IR) spectrum of the aragonite-$CaCO_3$ scale shows distinctive peaks at 709.1, 854.3, and 1486.7 cm^{-1} due to the C-O stretching and bending modes (Figure 2(c)). The sharp peak of X-ray diffractogram shown in Figure 2(d) is typical of a crystalline compound between 2θ of 25 to 50°. The short peak at 2θ of 35° was unexpected and suspected to be foreign materials of impurities in the sample. High crystalline nature indicates that $CaCO_3$ scale is in aragonite phase. This was confirmed by comparing the SEM micrograph of the sample in Figure 2(a) with that reported in Andritsos and Karabelas (2003).

3.2 WT monitoring

These readings were taken with the UT gauge externally to observe the change in WT with the progress of experiments. To ensure that subsequent measurements are taken on the same points, the same matrix as EFM pins was used. The results are shown in Figure 3(a) for baseline or reference WT, after the experiment to assess the deposition of scale, and after cleaning for wall loss measurement. The collected data revealed about 3% increase in the WT on average and a maximum increase of roughly 13% due to scaling. WT data collected after a thorough cleaning with the high-pressure washer was also compared with the baseline, revealing an average of 2.6% and a maximum 14% decrease. These measurements and observations are in conformance with the results reported in the literature (Ahmed et al. 2012, 2014; El-Gammal et al. 2010), that wall thinning are severe at the bend compared with other sections of the pipe owing to sudden changes in the flow direction and velocities. WT distribution at the center of the matrix outlay (Row 4) was plotted in Figure 3(b). It can be seen from the graph that the elbow section thickness increases after six months of exposure to the solution as a result of the scale deposit on the elbow wall. The WT reduced below the baseline after cleaning, with maximum thickness loss recorded around the middle of the elbow section (Row 4, point 7) of the pipe.

4 Modeling

In this section, firstly a background with the account of previous works related to corrosion modeling using NNs, their types and a comparison is given. This is followed by the description of data sets and NN used.

4.1 Background

In certain applications with complex processes such as corrosion, modeling is extremely complicated if not

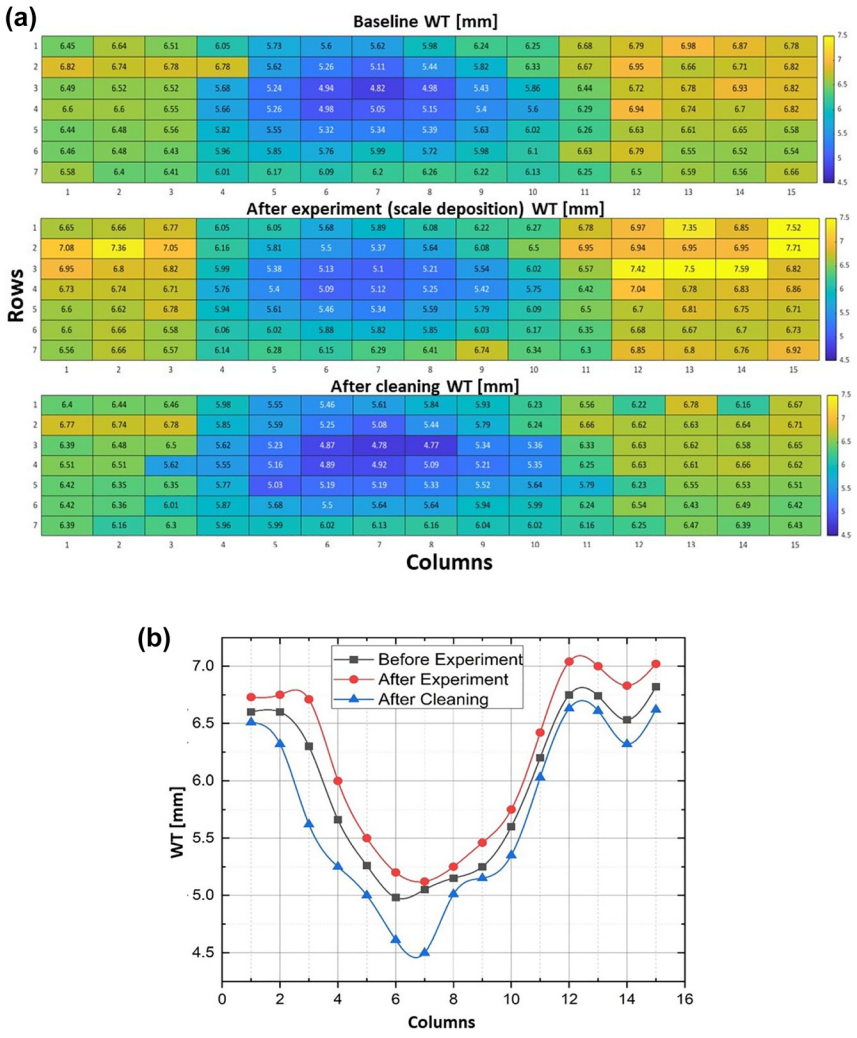

Figure 3: (a) Pipe WT color map before the experiment (top), after the experiment (middle) and after cleaning (bottom), (b) WT along row 4 of the pipe.

impossible and out of scope for traditional machine learning algorithms. NNs thus come into play, which are composed of neurons structured as input, output and single or multiple hidden layers. These layers form the core for learning hidden patterns in the available data. The number of hidden layers and neurons increases with the complexity of data. Interested readers are referred to Gurney (2018) for a detailed discussion on the basics, working and structure of NNs and left here for brevity.

A generalized regression neural network (GRNN), which is a probabilistic NN, was used by Ding et al. (2019) to model and predict the corrosion potential and current densities of CS samples in soils with different parameters which directly affect the corrosion rate of steel. Additionally, sensitivity analysis was done for the soil parameters. Pitting corrosion of SS 316L and EN 1.4404 was predicted using ANNs by Come et al. (2015) and Come et al. (2020), respectively, while considering environmental conditions. Specifically, later reported the results in marine environment. For pitting corrosion in SS, Petković et al. (2017) reported the results of using statistical and ANN modeling of AISI 316 LVM passivation process, which is aimed at building a passive protective layer on the steel surface for biomedical applications. Passivation parameters and pitting corrosion were used as parameters for the models. It was concluded that only ANN gave accurate predictions with low mean relative error compared with the statistical models. In another study, Paul (2016) reported on the pitting corrosion of SS 304 by seawater containing Cl in construction applications. Stochastic models were developed to predict the life of the corroding steel structure by taking into account the parameters that affect such a process. Specifically, the parameter that determines the onset of a leakage, i.e., maximum pit depth was modeled, and it was shown that it mainly depends on the electrochemical driving force and the time of elapse.

Recently, a comprehensive review was given in Li et al. (2020) regarding models for predicting stress corrosion cracking (SCC) specifically in structural materials used for

nuclear power plants. A number of references reported therein discussed and presented promising results of using ANNs for prediction. For specific case of SS 316L elbow with very high WT (approx. 80 mm) used in the nuclear reactors, Guo et al. (2017) discussed SCC propagation behavior through numerical simulations. Artificial defect was introduced at the internal surface to emulate a real crack.

4.2 Types and comparison of NNs

There are a number of NN types that can be used depending on the requirements of application (Gurney, 2018). Most commonly used are perceptron, feed-forward (FF), convolution, recurrent, Kohonen maps, and support vector machines (SVM). Perceptron is the most basic and smallest NN that does certain computations to detect features in the input data. Having a simple structure, they are only capable of implementing linearly separable problems. FF NNs on the other hand, find applications in more complex applications such as image processing, computer vision, and speech processing. They can be further classified into single and multilayered NNs, where the number of layers depends on the complexity. Apart from this flexibility, they can deal with data which contains significant noise, and are fast and easy to implement. In contrast, Convolution NNs are complex to design and slow in performance depending on the number of hidden layers. For sophisticated applications such as text auto-suggest, grammar checking, text-to-speech, and translation, Recurrent NNs are used because they are capable to model sequential data. However, training these NNs can be a challenging task. Kohonen maps are used in specialized applications to recognize patterns in the data, for instance in medical analysis to cluster data into different categories. SVMs, which are considered very robust for prediction applications, analyze the data for classification and regression analysis.

4.3 Description of the training set

The training inputs are ΔV, ΔI and T, each consisting of an array with 7 rows and 16 columns following the EFM pin pattern, collected at a flow rate of 2 m/s and concentration of 40 ppt. The readings were recorded hourly for approximately twenty days giving 482 measurements for each parameter. In order to model the input of the NN, each row was opened separately and concatenated with the next one such that 7 rows were transformed into a total of (16 columns 7 rows=) 112 series. Figure 4 shows the structure of the first two rows as an illustrative example of restructuring the data, where the hours became rows. This implied that the dimension of each training input was 482 by 112 per parameter, resulting in a 482 by 336 matrix for all the parameters.

The targets were remaining WT values measured between the pin locations, thus resulting in (15 spots between the pin columns 7 rows=) 105 samples of remaining WT measured for 482 h as well. Consequently, the dimension of the target was 482 by 105. The data was distributed such that 70% was used for training, 15% for validation and 15% was reserved for testing.

White noise with zero mean and standard deviation 5×10^{-3} mm was introduced into the target data (WT) during training, which was less than 0.1% of the nominal WT. This was done to prevent near-constant observations from terminating the training process.

4.4 NN for corrosion modeling

From NNs described above, FF NN was selected in this study due to the mentioned advantages. Moreover, it was planned to start with the basic NN after perceptron, i.e., FF network, and move to more sophisticated ones in case it failed to model the corrosion process. The model was trained under supervised learning, since the inputs and output training data sets were available. The input was denoted as $x_i, i = 1, 2, \ldots, n$

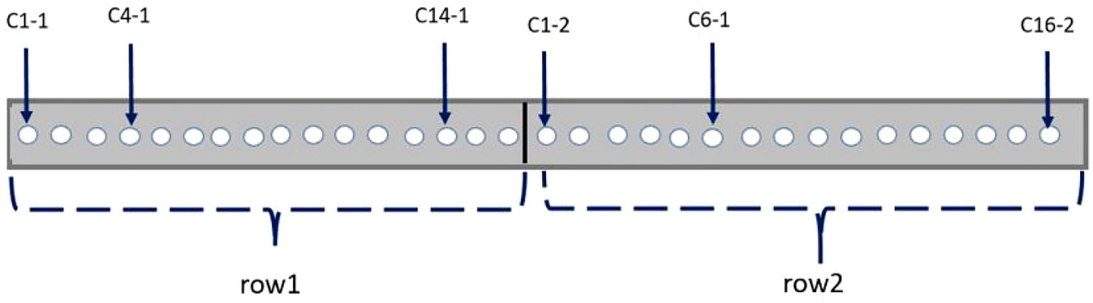

Figure 4: Illustration of data restructuring for NN training.

where n=336, each of length 482 resulting in the training input size of 336 by 482. The input features were subdivided into three, EI $(x_1, x_2, \ldots, x_{112})$, EV $(x_{113}, x_{114}, \ldots, x_{224})$, and T $(x_{225}, x_{226}, \ldots, x_{336})$. The targets were denoted by $y_j, j = 1, 2, \ldots, m$, where m = 105. Note that m and n are the number of sample features in the inputs and targets, respectively.

Neural Toolbox in MATLAB Demuth (2000), provides means of tuning the network parameters to enhance the learning accuracy. Some parameters, such as number of epochs can be chosen by default, while others like number of neurons and size of hidden layers can be selected by experience, or trial and error (Alahmed et al. 2019). To measure the performance of the model, mean absolute error (MAE), defined in Eq. (1) was adopted. Where N is the number of data points. This was reported by MATLAB toolbox at the end of the simulation.

$$\text{MAE} = \frac{\sum_{i=1}^{N} |\text{error}|}{N} \tag{1}$$

As a starting point, four and three hidden layers, each having ten neurons were considered based on experience, however, the NN over-learned and was not able to identify the WT for test data set in both cases. The number of layers was then reduced to one and various numbers of neurons were tried ranging from ten to fifty, however, the NN was not able to learn the corrosion behavior. Then the number of layers was increased to two, while keeping the number of neurons to ten. The validation performance of 0.53×10^{-3} was recorded at fourth epoch and R values of 0.99,967, 0.99,953 and 0.99,922 were obtained for training, validation and test sets, respectively. This indicated an excellent learning capability by the chosen model.

5 Results

To demonstrate the ability of the trained NN model, Figure 5(a)–(c) shows a comparison between the measured and estimated WT values on selected points. Clearly, both

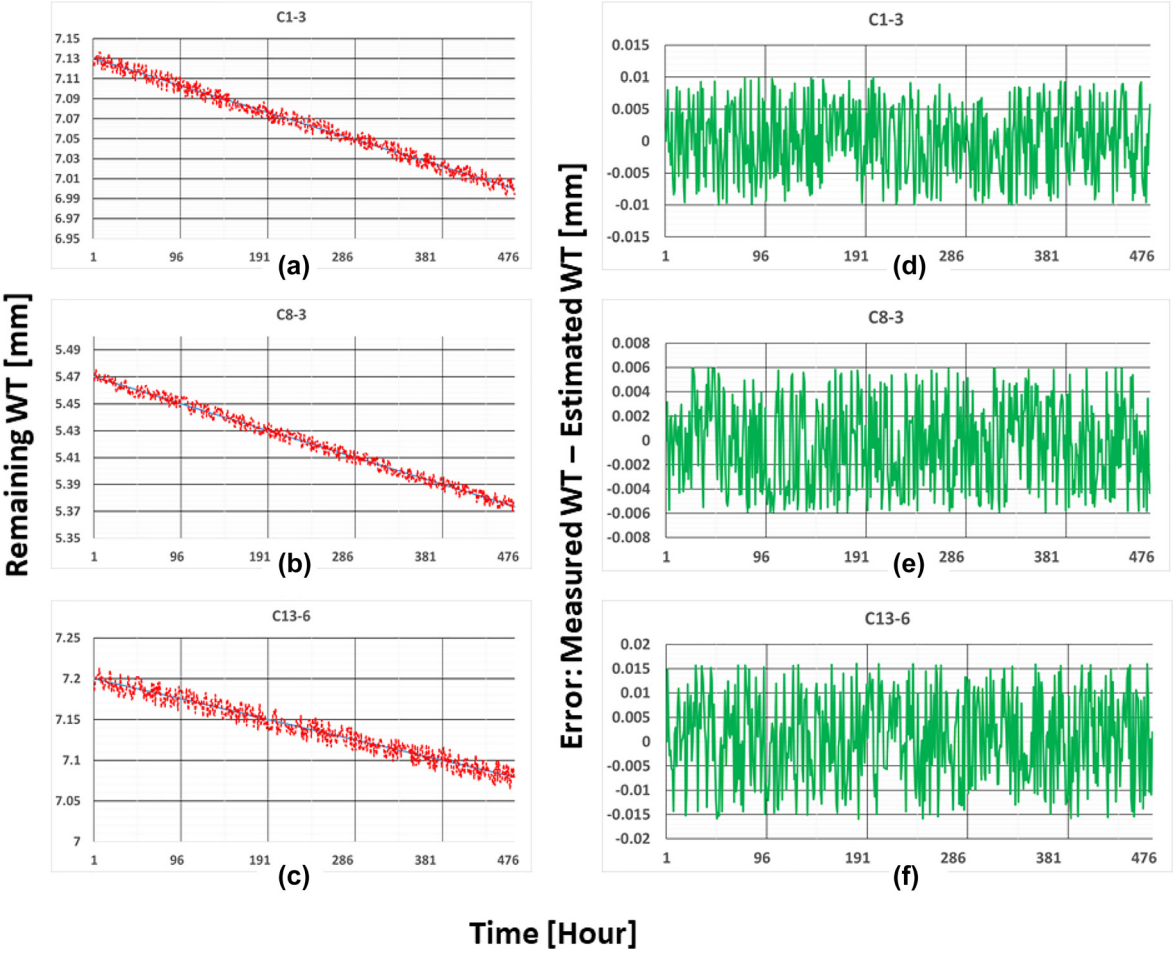

Figure 5: Measured versus estimated WT. (a) C1-3; (b) C8-3; (c) C13-6. Error between measured and estimated WT. (d) C1-3; (e) C8-3; (f) C13-6.

follow similar trends, sloping down from left to right for all columns, where the negative slope indicates a gradual decrease in the remaining WT with time. The variation seen in the estimated results is due to the addition of noise in the data. The average MAE for all the sixteen columns is 15×10^{-3} mm.

One of the selected points was around the center of the elbow (Figure 5(b)) and others were towards the elbow arms from both ends (a, c). Moreover, the remaining WT is shown for same row on the pipe but different columns, i.e., C1-3 and C8-3 to demonstrate that WT has higher values outside the elbow section as compared with the elbow, which is due to manufacturing.

Figure 5(d)–(f) shows the errors between measured and estimated WT values which has the maximum instantaneous value of 16×10^{-3} mm recorded at C13-6 corresponding to 0.27% of the nominal WT. Regarding estimation performance of the NN, it is worth mentioning that this was the maximum error recorded out of all the 112 points. The MAE for C1-3, C8-3, and C13-6 was recorded as 4.8, 3, and 7.8×10^{-3} mm, respectively.

These results show that the characteristics of the pipe corrosion can be thoroughly analyzed by using NN modeling, as seen from the above results. The findings suggest that a unique NN model could be developed for a specific pipe with better understanding of the elbow section, if all necessary data obtained from the principle of electric field mapping are available.

6 Conclusions

This paper presented first results of ANN modelling for wall loss in SS 316L elbow running saline water with known concentration and flow velocity. The measurement setup consisted of electric field mapping (EFM) pins to measure voltage and current readings, and temperature sensors. These observations were recorded for a period of 20 days and were used to train and test the ANN model for corrosion modeling. A detailed chemical and microscopic analysis of scales formed on the internal surface was also performed. The maximum MAE averaged over the entire elbow section was recorded as 15×10^{-3} mm, which is 0.25% of the nominal WT.

Future work will be focused on removing noise from the output (estimated WT) and also to extend the model to other flow and concentration values.

Author contribution: All the authors have accepted responsibility for the entire content of this submitted manuscript and approved submission.

Research funding: None declared.

Conflict of interest statement: The authors declare no conflicts of interest regarding this article.

References

Ahmed, W.H., Bello, M.M., El-Nakla, M., and Al-Sarkhi, A. (2012). Flow and mass transfer downstream of an orifice under flow accelerated corrosion conditions. Nucl. Eng. Des. 252: 52–67.

Ahmed, W.H., Bello, M.M., El-Nakla, M., Al-Sarkhi, A., and Badr, H.M. (2014). Experimental investigation of flow accelerated corrosion under two-phase flow conditions. Nucl. Eng. Des. 267: 34–43.

Alahmed, A.S., Taiwo, S.U., Abido, M.A., and Almuhaini, M.M. (2019). Intelligent flexible priority list for reconfiguration of microgrid demands using deep neural network. In: *IEEE Innovative Smart Grid Technologies-Asia (ISGT Asia)*. IEEE, Chengdu, China, pp. 21–24.

Andritsos, N. and Karabelas, A.J. (2003). Calcium carbonate scaling in a plate heat exchanger in the presence of particles. Int. J. Heat Mass Tran. 46: 4613–4627.

Choi, Y.-S., Nesic, S., and Ling, S. (2011). Effect of H2S on the CO2 corrosion of carbon steel in acidic solutions. Electrochim. Acta 56: 1752–1760.

Come, M.J.J., Turias, I.J., and Aguilar, J.J.R. (2015). A two-stage model based on artificial neural networks to determine pitting corrosion status of 316L stainless steel. Corrosion Rev. 34: 113–125.

Come, M.J.J., de la Luz Martín, M., Matres, V., and Baladés, J.D.M. (2020). The use of artificial neural networks for modelling pitting corrosion behaviour of EN 1.4404 stainless steel in marine environment: data analysis and new developments. Corrosion Rev. 38: 339–353.

Demuth, H. (2000). Neural network toolbox TM 6 user's guide. Network 9: 259–265.

Ding, L., Rangaraju, P., and Poursaee, J. (2019). Application of generalized regression neural network method for corrosion modeling of steel embedded in soil. Soils Found. 59: 474–483.

El-Gammal, M., Mazhar, H., Cotton, J.S., Shefski, C., Pietralik, J., and Ching, C.Y. (2010). The hydrodynamic effects of single-phase flow on flow accelerated corrosion in a 90-degree elbow. Nucl. Eng. Des. 240: 1589–1598.

Guo, S., Han, E.H., Wang, H., Zhang, Z., and Wang, J. (2017). Life prediction for stress corrosion behavior of 316L stainless steel elbow of nuclear power plant. Acta Metall. Sin. 53: 455–464.

Gurney, K. (2018). *An introduction to neural networks*, 1st ed. CRC Press, London.

Heidary, R., Gabriel, S.A., Modarres, M., Groth, K.M., and Vahdati, N. (2018). A review of data-driven oil and gas pipeline pitting corrosion growth models applicable for prognostic and health management. Int. J. Prognostics Health Manag. 9: 1–13.

Hu, X. and Neville, A. (2009). CO2 erosion–corrosion of pipeline steel (API X65) in oil and gas conditions—a systematic approach. Wear 267: 2027–2032.

Khan, R., Ya, H.H., and Pao, W. (2019). An experimental study on the erosion-corrosion performance of AISI 1018 carbon steel and AISI 304L stainless steel 90-degree elbow pipe. Metals 9: 1260.

Li, Z., Lu, Y., and Wang, X. (2020). Modeling of stress corrosion cracking growth rates for key structural materials of nuclear power plant. J. Mat. Sc. 55: 439–463.

Papavinasam, S., Revie, R.W., Friesen, W.I., Doiron, A., and Panneerselvan, T. (2006). Review of models to predict internal

pitting corrosion of oil and gas pipelines. Corrosion Rev. 24: 173–230.

Paul, S. (2016). Modeling unpredictable failures of 304 construction material in seawater by pitting corrosion and simulate chloride ion distribution by finite element method. Multidiscip. Model. Mater. Struct. 12: 543–557.

Petković, D.L., Madić, M.J., and Radenković, G.M. (2017). The effects of passivation parameters on pitting potential of biomedical stainless steel. Chem. Ind. Chem. Eng. Q. 23: 121–129.

Shadley, J.R., Shirazi, S.A., Dayalan, E., Ismail, M., and Rybicki, E.F. (1996). Erosion-corrosion of a carbon steel elbow in a carbon dioxide environment. Corrosion 52: 714–723.

Vanaei, H.R., Eslami, A., and Egbewande, A. (2017). A review on pipeline corrosion, in-line inspection (ILI), and corrosion growth rate models. Int. J. Pres. Ves. Pip. 149: 43–54.

Wan, T. and Saito, S. (2018). Flow-accelerated corrosion of type 316L stainless steel caused by turbulent lead–bismuth eutectic flow. Metals 8: 627.

Xie, M. and Tian, Z. (2018). A review on pipeline integrity management utilizing in-line inspection data. Eng. Fail. Anal. 92: 222–239.

Zeng, L., Guo, X.P., Zhang, G.A., and Chen, H.X. (2018). Semiconductivities of passive films formed on stainless steel bend under erosion-corrosion conditions. Corrosion Sci. 144: 258–265.